Wall-modeled LES of flow over a Gaussian bump

Prahladh S. Iyer*
National Institute of Aerospace, Hampton, VA 23666

Mujeeb R. Malik†
NASA Langley Research Center, Hampton, VA 23681

We perform wall-modeled large eddy simulations (WMLES) of turbulent flow over a Gaussian-shaped bump geometry, to assess its performance in the accelerating and separation regions of the flow. The flow conditions are based on the ongoing CFD validation experiments of Slotnick [NATO STO-MP-AVT-307, 2019]. The oncoming flow Mach number is 0.176, and two Reynolds numbers are simulated that are about 10000 and 36000 based on boundary layer thickness upstream of the bump. Preliminary Reynolds-averaged Navier-Stokes simulations are first performed to assess the effects of Mach number, Reynolds number, tunnel top and side wall effects. Finally, WMLES results with an equilibrium wall model will be presented at two Reynolds numbers to assess their performance for this flow by making detailed comparisons with available experimental and higher-fidelity numerical data.

I. Introduction

High fidelity simulation methodologies are required to improve our understanding of flows over complex geometries. Computational Fluid Dynamics (CFD) can play a critical role in the design of aerospace vehicles owing to the detailed information regarding the flow physics and statistics it can provide. Reynolds-averaged Navier-Stokes (RANS)-based methods are currently widely used for high Reynolds number turbulent flows but are not accurate for complex flows involving separation. High fidelity Direct Numerical Simulation (DNS) and Large Eddy Simulation (LES) methods, while accurate, are infeasible for realistic flight Reynolds number flows. Performing a wall resolved LES simulation of a full powered aircraft configuration in the full flight envelope is a grand challenge problem in the NASA CFD Vision 2030 study [1], which is not expected to be realized in the near-future.

The wall-modeled LES approach, in which the near-wall region is modeled with RANS, while the majority of the length scales away from the wall are resolved using LES, is a reasonable compromise between accuracy and computational cost. Wall-modeled LES can further be classified into (i) stress-based WMLES, and (ii) hybrid RANS/LES methods such as Improved Delayed Detached Eddy Simulation (IDDES). In the stress-based WMLES approach, the computational grid is coarse in the wall-normal and wall-parallel directions, thus requiring the regular no-slip boundary condition to be supplemented by a wall shear stress and heat flux/ temperature boundary conditions. See Cabot & Moin [2], Piomelli & Balaras [3], Larsson et al. [4] and Bose & Park [5] for overviews of stress-based WMLES. In IDDES, the grid is very fine in the wall-normal direction but coarse in the wall-parallel direction thus requiring the LES eddy viscosity to be replaced by a RANS eddy viscosity where the majority of the turbulence is modeled. See Spalart [6], Deck [7], Spalart et al. [8] and Shur et al. [9] for an overview of the DES-based approach. In this study, we focus on the stress-based WMLES approach, which is implied when we refer to WMLES in the rest of the paper.

Wall-modeled large eddy simulation (WMLES) and hybrid RANS/LES methods are becoming increasingly popular for high Reynolds number turbulent flow configurations with separation due to their potential to be more accurate compared to Reynolds-averaged Navier-Stokes simulations (RANS), which are the current industry standard. While the RANS technique models all of the turbulence, the WMLES technique resolves a significant portion of the energy-carrying eddies away from the wall. Thus, grid refinement in WMLES is likely to lead to more accurate predictions, while the modeling error, which dominates in RANS, is independent of the grid resolution. WMLES has shown good promise for a variety of flow configurations involving flow separation [9–26]. Nevertheless, the current framework and models used in WMLES are far from perfect; further understanding and improvements are necessary to enable their use for complex industrial applications [1].

*Research Scientist, AIAA Senior Member.
†Senior Aerodynamicist, Computational AeroSciences Branch, MS 128, AIAA Fellow.

Careful CFD validation experiments of flow over a Gaussian bump configuration are being performed by Williams et al. [27] to assess the predictive ability of various simulation approaches, i.e., RANS, WMLES and Direct Numerical Simulation (DNS). The experimental conditions were chosen based on close collaboration with experts at Boeing, to be a challenging test case for turbulence modeling approaches. We use an unstructured finite volume solver with the equilibrium wall model to evaluate its performance for the chosen configuration. Most previous WMLES studies involving separation have been restricted to a single Reynolds number (Re), but here, we wish to examine the predictions at two Re, with the smaller one accessible to DNS for detailed comparisons. Uzun & Malik [28] have performed DNS for the same configuration with a detailed analysis of the flow physics on the favorable and adverse pressure gradient regions of the flow. The WMLES framework has been used in previous studies such as flow over a wall-mounted hump [15], which has shown promise in predicting separated flows.

The paper is organized as follows. The details of the flow solver and wall model are briefly discussed in Section II. The flow conditions, configuration, grid and simulation details are discussed in Section III. Assessment of compressibility and tunnel wall effects using RANS are described in Section IV, while the WMLES results for the spanwise periodic configuration at two Reynolds numbers are presented in Section V. A brief summary in Section VI concludes the paper.

II. Numerical Details

The Charles solver* is used in the simulations. The compressible solver discretizes the Navier-Stokes equations on unstructured grids using a cell-centered finite-volume methodology. The baseline solver is second-order accurate in space for unstructured grids with an explicit third-order Runge-Kutta time advancement scheme. Numerical stability is achieved by blending with an upwind flux in regions of poor grid quality. Further details about the numerics can be found in Khaligi et al. [29] and Park & Moin [30]. The constant coefficient Vreman model is used to model the subgrid terms, and the equilibrium wall model [31] is used to prescribe the wall shear-stress in this study. The equilibrium wall model is technically only valid for attached regions of the flow as it does not capture nonequilibrium effects in accelerating and separated regions of the flow. Hence, the accuracy of the prediction in nonequilibrium regions is dependent on how much of these effects are captured by the outer layer (resolved by LES) and the grid resolution in the region, and the effect of skin-friction on the outer layer in such regions. It uses a mixing-length based turbulent eddy viscosity in the wall model equations [31]. We have previously used the same setup with the equilibrium wall model to study two-dimensional (in the mean) separated flows [15, 16, 18, 24], and obtained good comparison with available experimental data.

III. Problem Description

The experimental configuration of Slotnick [32] consists of a symmetric Gaussian-shaped bump in the center of the wind tunnel ($z = 0$) with a length and width L, that extends to the sides of the tunnel ($z/L = \pm 0.5$). It is attached to a flat plate section both upstream and downstream of the bump ($|x/L| > 0.5$), and tapered along the spanwise direction (z) to minimize side-wall interference effects. The shape of the bump can be described by the following equation:

$$y(x,z) = \frac{h_0}{2} e^{-\left(\frac{x}{x_0}\right)^2} \left[1 + \mathrm{erf}\left(\frac{\frac{L}{2} - 2z_0 - |z|}{z_0}\right)\right] \tag{1}$$

Here, x, y and z are the streamwise, wall-normal and spanwise directions of the oncoming boundary layer, and L is the width of the tunnel (which is also equal to the length of the bump). The constants $x_0 = 0.195L$, $z_0 = 0.06L$ and $h_0 = 0.085L$ are used, and the corresponding shape of the bump in the $x - y$ and $y - z$ planes are shown in Figure 1. The term in the square brackets in Equation 1 is unity at $z = 0$, which is used for the spanwise-periodic simulations in this study. Experiments are carried out by Williams et al. [27] for this configuration for CFD validation purposes. The experimental Reynolds number ($Re_L = u_\infty L/\nu_\infty$) ranges from $0.69 - 3.6$ million in the tunnel, while results were reported for $Re_L = 1.3 - 3.5$ million in Williams et al. [27] which corresponds to a freestream Mach number of $0.07 - 0.17$. Our simulations are performed at a freestream Mach number of 0.176, and $Re_L = 1$ and 3.6 million. The lower Reynolds number corresponds to the value used by Uzun & Malik [28] in their DNS of this flow configuration, which is used for comparison and validation.

Most of the WMLES results reported are for the spanwise periodic case, with a spanwise domain width of $L_z/L = 0.04$. The inflow is placed at $x/L = -0.8$, and outflow is at $x/L = 2.0$. Mean flow taken from RANS (see

*Cascade Technologies, Webpage: `http://www.cascadetechnologies.com` [Last accessed: May 25, 2020]

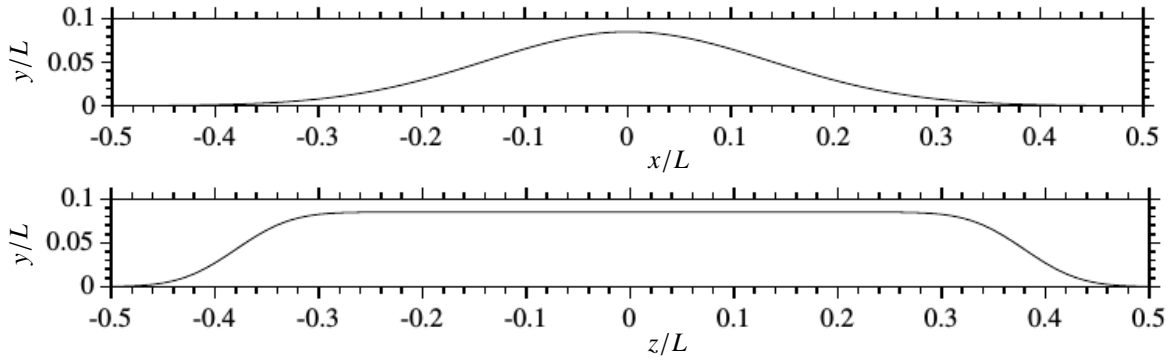

Fig. 1 The shape of the bump in the $x-y$ plane at the symmetry plane $z = 0$ (top), and $y-z$ plane at the center of the bump $x = 0$ (bottom), are shown. These figures are reproduced from Williams et al. [27]

Section IV) using the Spalart-Allmaras (SA) model with rotation and curvature (RC) correction, and the quadratic constitutive relationship for turbulent stress (QCR) is superimposed with synthetic fluctuations using the method of Shur et al. [33], which we have previously used for supersonic shock/turbulence interaction [24, 34] and the NASA juncture flow problem[35]. Sponge boundary conditions (BC) are imposed for $x/L > 1.0$ to minimize reflections from the outflow. The top wall is placed at $y/L = 0.5$ similar to the experiment, but an inviscid slip wall BC is imposed there. For the full 3D simulation, the side walls are also treated as inviscid slip walls. The effect resolving the viscous tunnel wall boundary layers (top and side walls) appears to be small for the statistics in the symmetry plane as discussed in Section IV. The equilibrium wall model is applied on the bottom wall with an adiabatic thermal condition. A snapshot of the coarse grid in the symmetry plane is shown in Figure 2.

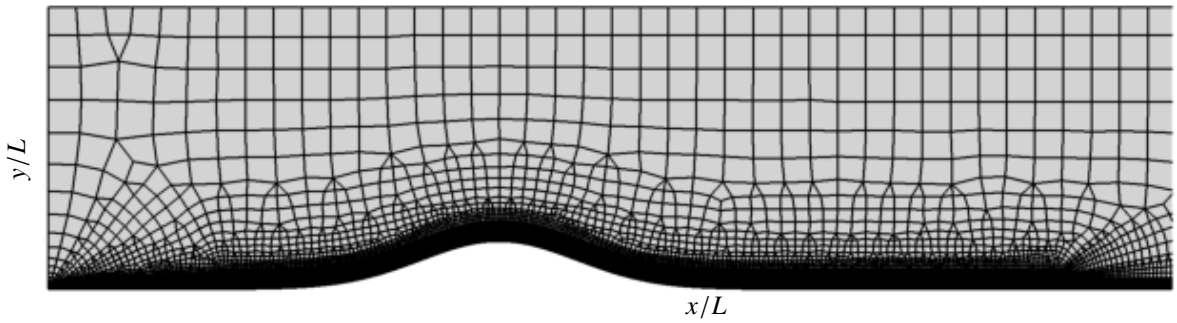

Fig. 2 The coarse grid used in WMLES is shown in the symmetry plane $z = 0$.

The boundary layer thickness of the oncoming turbulent boundary layer (δ_i) is $\approx 0.01L$ at $x/L \approx -0.65$, which is used as a reference to construct the WMLES grid. The coarse grid contains about 10 points per boundary layer thickness (ppd), and is mostly isotropic, i.e., $\Delta x = \Delta y = \Delta z$. The wall-normal spacing near the inflow is reduced to maintain 10 ppd resolution. The grid spacing is $0.001L$ and $0.0005L$ for the coarse and medium grids used here, which contain about 2 and 16 million grid points for an $L_z/L = 0.04$. The coarse grid spacing of $0.001L$ corresponds to a viscous wall spacing of $\approx 50-100$ and $150-300$, for $Re_L = 1$ and 3.6 million, respectively. A finer grid containing 25 million grid points (for $L_z/L = 0.04$) is further refined by a factor of 2 over the bump, when compared to the 16 million grid. The coarse grid for the full 3D configuration contains 87 million points. The minimum wall-normal spacing over the bump is $0.001L$ and $0.00025L$ for the coarse and medium grids. Time-filtering of the wall model input is turned on for the cases that used the first grid point as the exchange location based on the recommendation of Yang et al. [36].

Instantaneous vorticity magnitude contours are shown for the coarse spanwise periodic grid at $Re_L = 1$ million in Figure 3 to illustrate the main features of this flow. The upstream turbulent boundary layer first experiences a favorable pressure gradient until the apex of the bump, beyond which it encounters adverse pressure gradient leading to possible

flow separation. Instantaneous isocontours of the $Q-$criterion is shown in Figure 4 for the coarse grid 3D simulation at $Re_L = 1$ million to depict the vortices captured by the grid resolution. Coherent hairpin eddies are visible upstream, above and downstream of the bump indicating that the outer layer appears to be qualitatively captured by this grid.

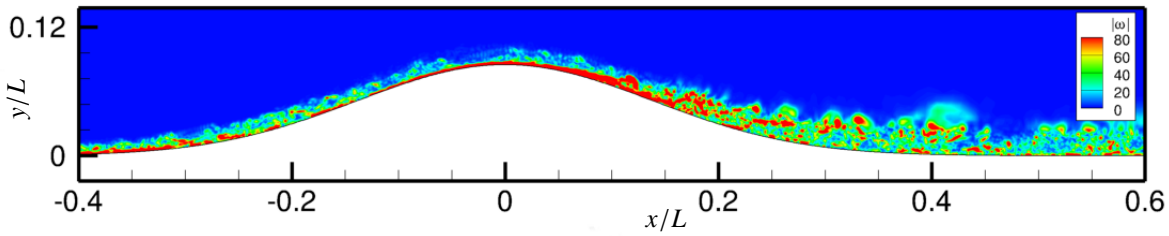

Fig. 3 Instantaneous vorticity magnitude contours ($|\omega|$) are shown for the spanwise periodic coarse WMLES at $Re_L = 1$ million.

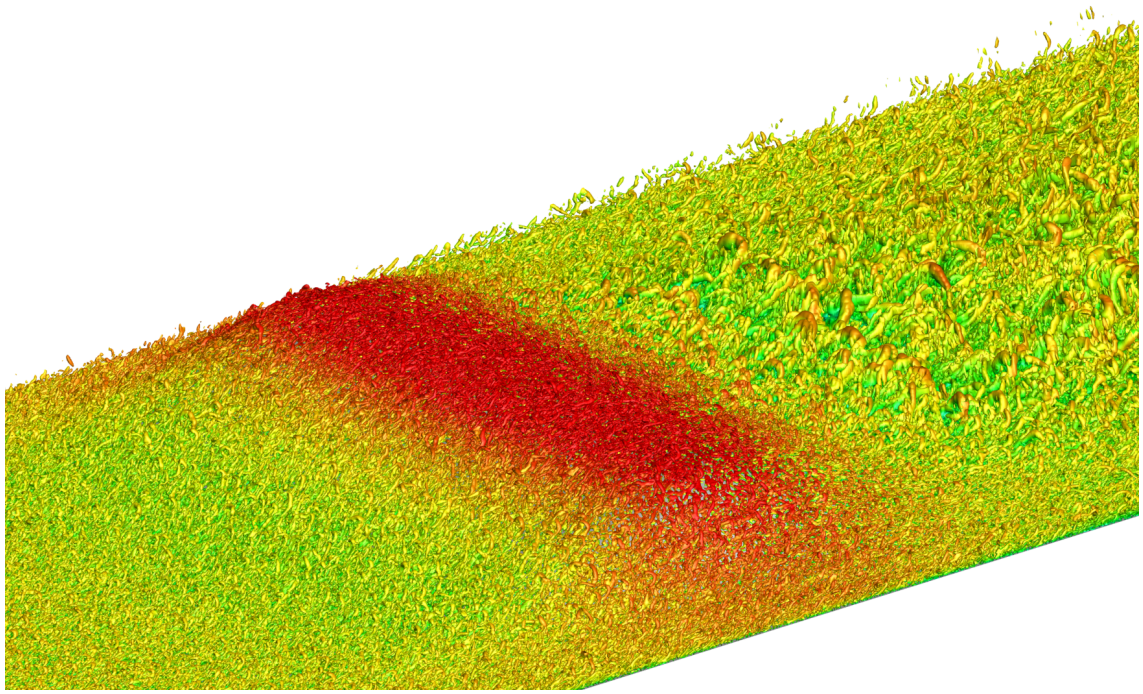

Fig. 4 Isocontours of $Q-$criterion are shown for the 3D coarse grid WMLES at $Re_L = 1$ million to depict the vortical features captured. Turbulent eddies are visible upstream, above and downstream of the bump.

IV. Compressibility and Tunnel Wall Effects using RANS

We evaluate the effect of compressibility and viscous tunnel wall effects for the 2D configuration using SA RANS. FUN3D V13.1 [37] was used for these computations. The grid used is wall-resolved with a $\Delta y_w^+ < 1.0$ (for top and bottom walls), and a no-slip, isothermal BC is imposed at the wall. All the reported results have residuals converged below 10^{-12}. The no-slip bottom wall begins at $x/L = -1$. The effect of Mach number on C_f is reported in Figure 5 for $Re_L = 1$ million and $M_\infty = 0$, 0.01 and 0.176 (with 0 denoting an incompressible simulation), using a viscous no-slip top wall. It can be seen that compressibility has a small effect on the separation bubble size. The figure also shows the effect of the viscous top wall boundary layer by comparing with a simulation using an inviscid slip BC at the top. It is

seen that the difference is negligible, indicating that the effect of viscous boundary layer on the top tunnel wall is small for this flow.

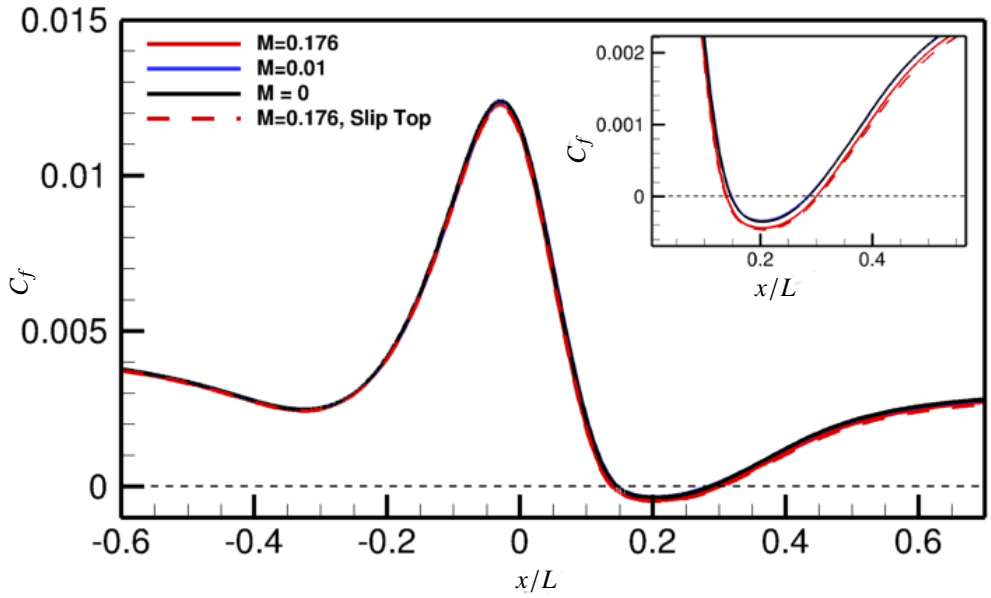

Fig. 5 The wall skin friction C_f variation for the 2D simulation using SA RANS for $Re_L = 1$ million is shown depicting the effect of compressibility and top wall boundary condition.

We report RANS calculations for the full 3D configuration, and a 2D slice to evaluate the effect of the three dimensional effects on the flow. For 3D flows involving separation, the quadratic constitutive relationship (QCR) for the turbulent stress significantly improves the accuracy of predictions [38] for RANS, especially, if the separation is dominated by turbulent stress gradients. Thus, we report results using the regular SA model (linear stress/strain relationship), and the SA-RC-QCR2000 model (QCR with rotation/curvature correction). See the NASA Turbulence Modeling Website[†] for the details of SA-RC-QCR2000 model. The variation of C_f and C_p for the bottom wall in the symmetry plane ($z = 0$) is shown in Figure 6. The effect of 2D versus 3D simulation, and the SA linear versus SA-RC-QCR2000 model is reported for the two Re_L of 1 and 3.6 million studied here. For the $Re_L = 1$ million case, spanwise periodic DNS results of Uzun & Malik [28] are also shown. The results indicate that for statistics in the symmetry plane, the effect of simulating the full 3D configuration is small. However, the SA and SA-RC-QCR2000 predictions show significant differences, with the latter predicting a larger separation bubble. The SA linear model is closer to the DNS for this case. The 3D simulations also show a reduced C_p at the apex of the bump due to the increased blockage of the tunnel walls. Preliminary coarse grid WMLES results also seem to qualitatively agree with the observations from RANS regarding the effect of simulating the full 3D configuration. Time-averaged wall pressure (C_p) variation in the symmetry plane for the spanwise periodic, and full 3D configuration from WMLES is shown for $Re_L = 1$ million in Figure 7.

V. Results

WMLES results are shown for the spanwise periodic simulations for $Re_L = 1$ and 3.6 million. The results from the coarse, medium and fine grids are shown, which contain 2, 16 and 25 million grid points, respectively. Also shown are the 2D RANS results using the SA-RC-QCR2000 model, and DNS of Uzun & Malik [28] for the lower Re_L case. Figure 8 shows the variation of C_f and C_p for $Re_L = 1$ million case. The WMLES results are sensitive to the grid resolution used, and the 25 million grid result agrees best with the DNS result, overall. A slight overprediction of C_f upstream of the bump is observed for the 16 and 25 million grid results. The variation of time-averaged velocity, normal and shear turbulent stress at $x/L = -0.4, -0.2$ and 0.2 are shown for $Re_L = 1$ million in Figure 9. These stations

[†]https://turbmodels.larc.nasa.gov/spalart.html, Last accessed: 25 May 2020

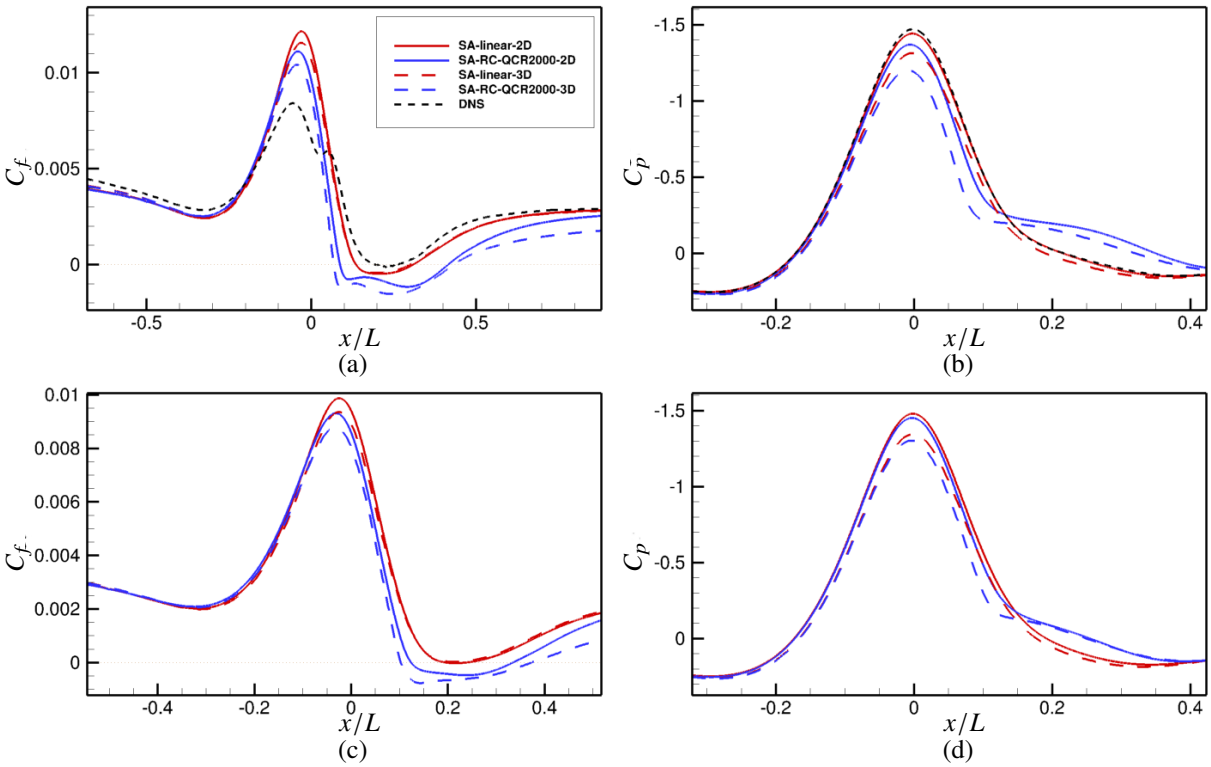

Fig. 6 The variation of wall skin friction (a,c) and pressure (b,d) predicted by SA and SA-RC-QCR2000 RANS models for Re_L = 1 million (a,b) and 3.6 million (c,d). The results are reported in the symmetry plane ($z = 0$) for the 3D simulation, and compared to the 2D case.

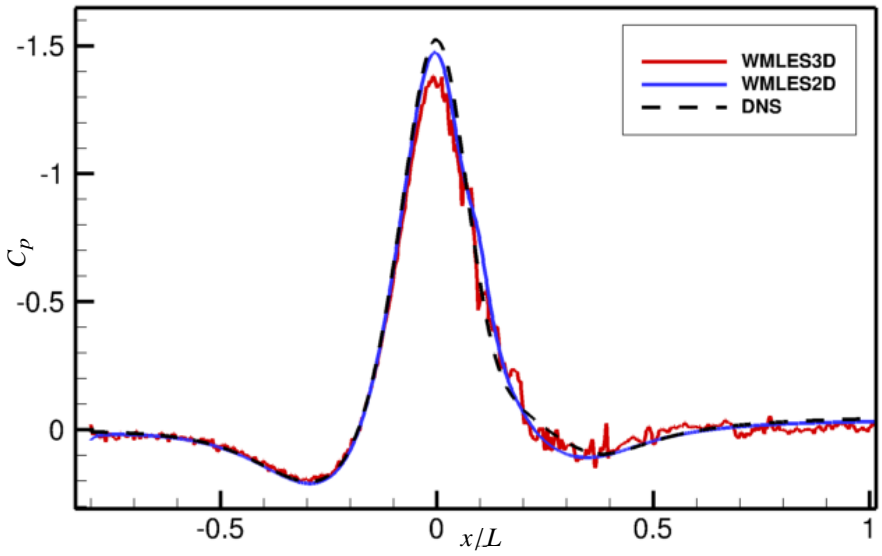

Fig. 7 The variation of mean wall pressure (C_p) in the symmetry plane ($z = 0$) is shown for the coarse full 3D, and spanwise periodic WMLES.

correspond to the nearly-zero pressure gradient (ZPG) upstream turbulent boundary layer region, accelerating and separation regions, respectively. At $x = -0.2$, the velocity and normal turbulent stress are qualitatively similar to the upstream ZPG station, but the turbulent shear stress profile is significantly altered due to the curvature and pressure gradient effects. At $x/L = 0.2$, the profiles resemble a separated shear layer region, with the peak turbulent stresses away from the wall. Here again, we observe that the results improve with increased grid resolution, with the finest grid (25 million) showing the best agreement with DNS.

The variation of C_f and C_p are shown for the spanwise periodic WMLES at $Re_L = 3.6$ million in Figure 10. The same grids used for the lower Re_L case are also used here, and so have lower grid resolutions in viscous units (by approximately a factor of 3). The results do not show any separation in the mean for this Re_L, with a decreased tendency to separate as the grid resolution increases. Further analysis of these results at both Re_L are currently underway to interpret results, and determine the optimal grid resolution required to capture the various aspects of this flow.

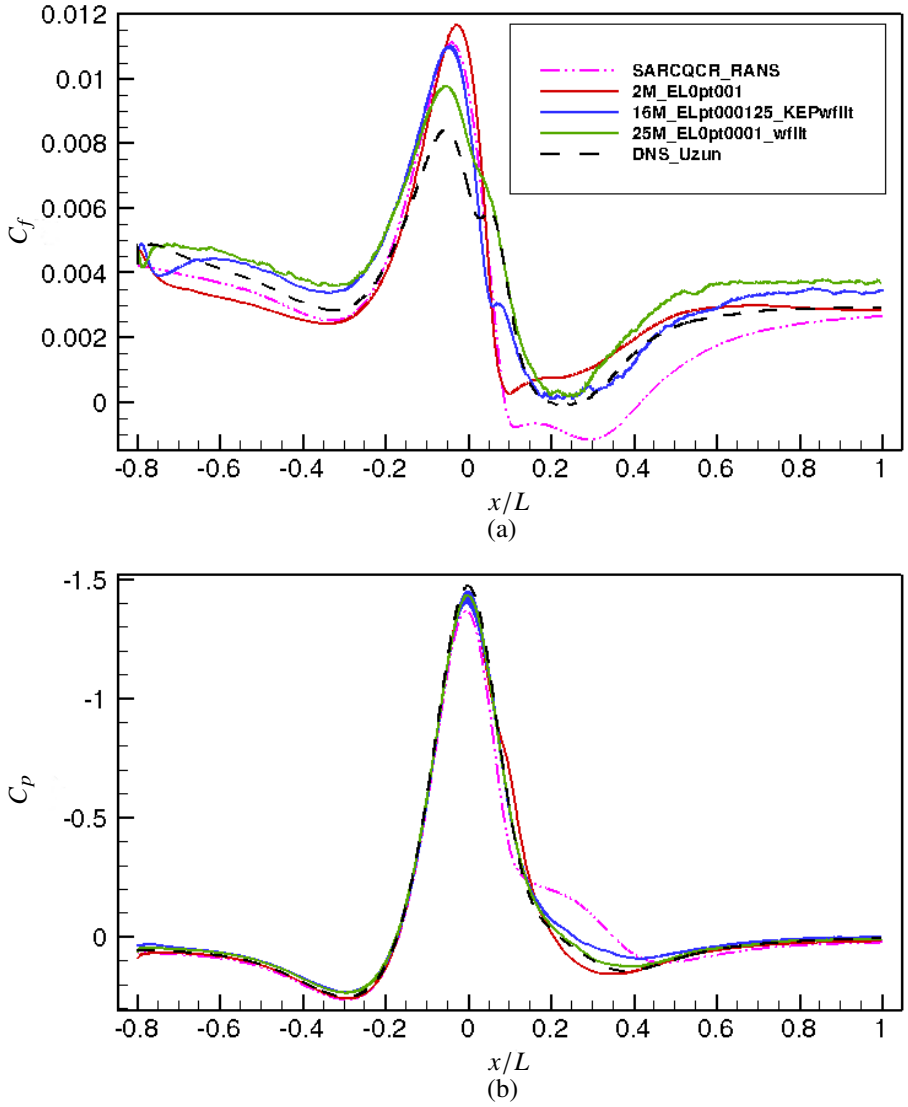

Fig. 8 The variation of wall skin friction (a) and pressure (b) is shown for the $Re_L = 1$ million spanwise periodic WMLES at different grid resolutions. Also included are the SA-RC-QCR2000 result, and the DNS result of Uzun & Malik [28].

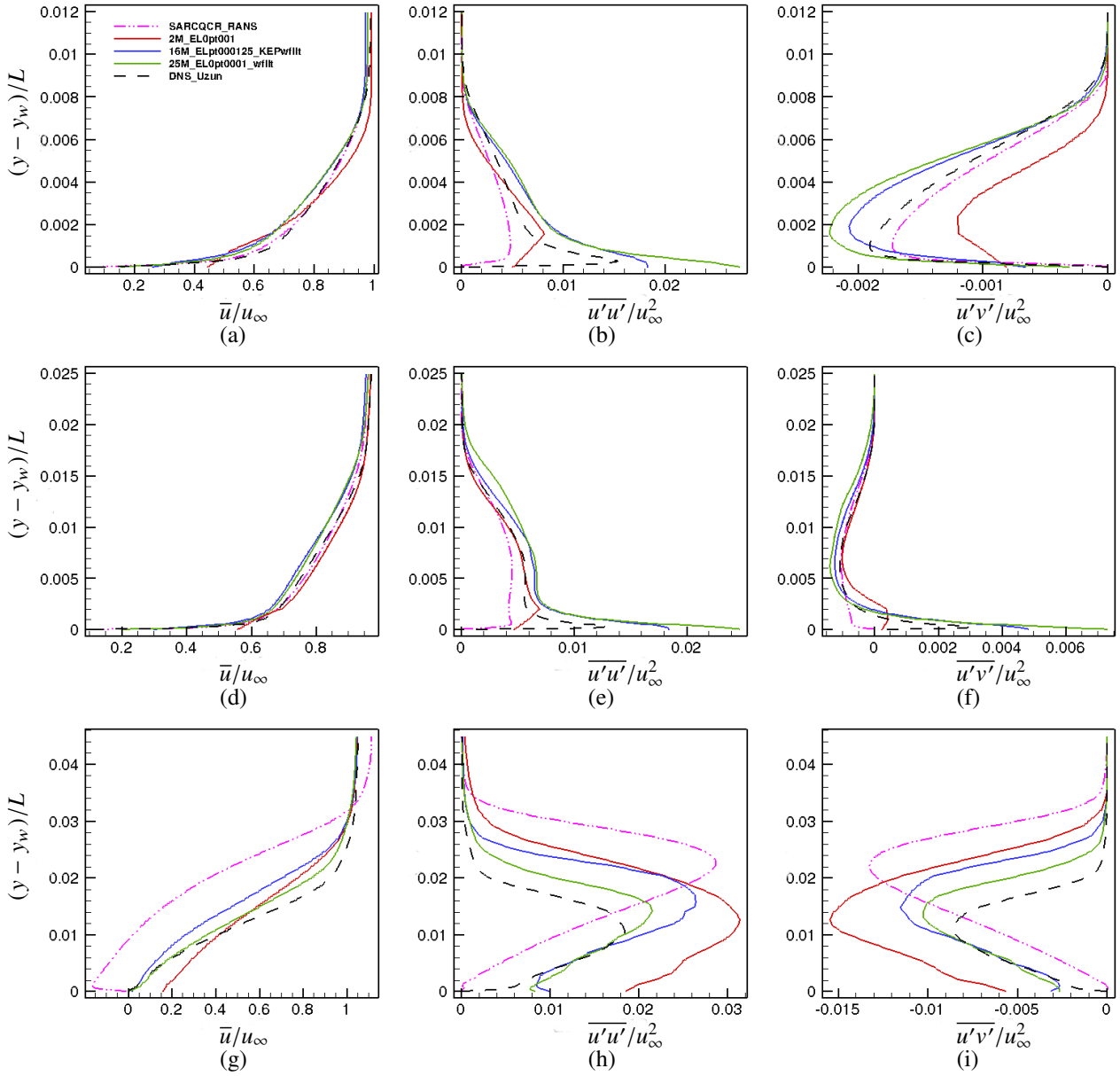

Fig. 9 Profiles of time-averaged velocity ($\overline{u}$), turbulent normal ($\overline{u'u'}$) and shear stress($\overline{u'v'}$) at constant horizontal stations corresponding to $x/L = -0.6$ (a,b,c), -0.2 (d,e,f) and 0.2 (g,h,i). Note that the top, center and bottom locations also correspond to nearly-zero, favorable and adverse pressure gradient regions.

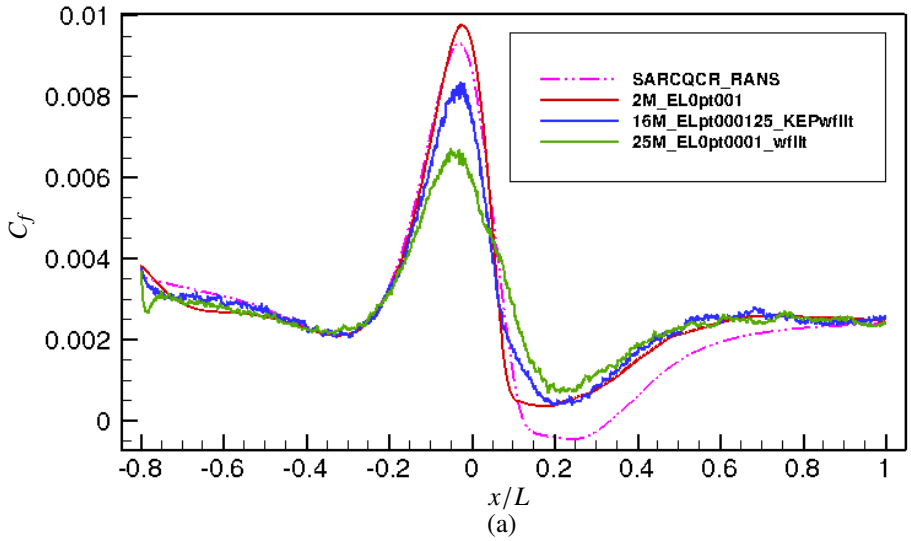

Fig. 10 The variation of wall skin friction (a) and pressure (b) is shown for the $Re_L = 3.6$ million spanwise periodic WMLES at different grid resolutions. Also included are the SA-RC-QCR2000 result for comparison.

VI. Summary and Future Work

We performed wall-modeled large eddy simulation (WMLES) of the flow past a Gaussian bump at two Reynolds numbers of 1 and 3.6 million based on the length of the bump. Reynolds-averaged Navier-Stokes (RANS) simulations were used to understand the effects of compressibility and viscous tunnel wall effects for this configuration. RANS and coarse grid WMLES appear to indicate that statistics in the tunnel symmetry plane are not significantly different between a spanwise periodic and full 3D configuration. The effect of grid resolution is assessed in WMLES, with the finest grid agreeing reasonably well with DNS for the lower Re_L case. The final paper will report further analysis of the results presented here, and finer grid and full 3D configuration results for the higher Re_L case.

Acknowledgments

This research is sponsored by the NASA Transformational Tools and Technologies (TTT) Project of the Transformative Aeronautics Concepts Program under the Aeronautics Research Mission Directorate. The work of the first author was sponsored by NASA under cooperative agreement NNL09AA00A. We thank Cascade Technologies for providing the Charles solver and consultation in use of the code.

References

[1] Slotnick, J., Khodadoust, A., Alonso, J., Darmofal, D., Gropp, W., Lurie, E., and Mavriplis, D., "CFD vision 2030 study: a path to revolutionary computational aerosciences," NASA-CR-2014-218178, 2014.

[2] Cabot, W., and Moin, P., "Approximate wall boundary conditions in the large-eddy simulation of high Reynolds number flow," *Flow, Turbulence and Combustion*, Vol. 63, No. 1–4, 2000, pp. 269–291.

[3] Piomelli, U., and Balaras, E., "Wall-layer models for large-eddy simulations," *Annual Review of Fluid Mechanics*, Vol. 34, No. 1, 2002, pp. 349–374.

[4] Larsson, J., Kawai, S., Bodart, J., and Bermejo-Moreno, I., "Large eddy simulation with modeled wall-stress: recent progress and future directions," *Mechanical Engineering Reviews*, Vol. 3, No. 1, 2016, pp. 15–00418.

[5] Bose, S. T., and Park, G. I., "Wall-modeled large-eddy simulation for complex turbulent flows," *Annual Review of Fluid Mechanics*, Vol. 50, No. 1, 2018.

[6] Spalart, P. R., "Detached-eddy simulation," *Annual Review of Fluid Mechanics*, Vol. 41, 2009, pp. 181–202.

[7] Deck, S., "Zonal-detached-eddy simulation of the flow around a high-lift configuration," *AIAA journal*, Vol. 43, No. 11, 2005, pp. 2372–2384.

[8] Spalart, P. R., Deck, S., Shur, M., Squires, K., Strelets, M. K., and Travin, A., "A new version of detached-eddy simulation, resistant to ambiguous grid densities," *Theoretical and computational fluid dynamics*, Vol. 20, No. 3, 2006, pp. 181–195.

[9] Shur, M. L., Spalart, P. R., Strelets, M. K., and Travin, A. K., "A hybrid RANS-LES approach with delayed-DES and wall-modelled LES capabilities," *International Journal of Heat and Fluid Flow*, Vol. 29, No. 6, 2008, pp. 1638–1649.

[10] Balakumar, P., Park, G., and Pierce, B., "DNS, LES, and wall-modeled LES of separating flow over periodic hills," *Proceedings of the Summer Program, Center for Turbulence Research, Stanford University*, 2014, pp. 407–415.

[11] Park, G. I., and Moin, P., "An improved dynamic non-equilibrium wall-model for large eddy simulation," *Physics of Fluids*, Vol. 26, No. 1, 2014, p. 015108.

[12] Bermejo-Moreno, I., Campo, L., Larsson, J., Bodart, J., Helmer, D., and Eaton, J. K., "Confinement effects in shock wave/turbulent boundary layer interactions through wall-modelled large-eddy simulations," *Journal of Fluid Mechanics*, Vol. 758, 2014, pp. 5–62.

[13] Yang, X., Sadique, J., Mittal, R., and Meneveau, C., "Integral wall model for large eddy simulations of wall-bounded turbulent flows," *Physics of Fluids*, Vol. 27, No. 2, 2015, p. 025112.

[14] Duda, B., and Fares, E., "Application of a Lattice-Boltzmann method to the separated flow over the NASA hump," AIAA Paper 2016–1836, 2016.

[15] Iyer, P. S., and Malik, M. R., "Wall–modeled large eddy simulation of flow over a wall–mounted hump," AIAA Paper 2016–3186, 2016.

[16] Iyer, P. S., Park, G. I., and Malik, M. R., "A comparative study of wall models for LES of turbulent separated flow," Proceedings of the 2016 Summer Program, Center for Turbulence Research, Stanford University, 2016.

[17] Park, G. I., "Wall-modeled large-eddy simulation of a high Reynolds number separating and reattaching flow," *AIAA Journal*, 2017, pp. 3709–3721.

[18] Iyer, P. S., Park, G. I., and Malik, M. R., "Wall–modeled large eddy simulation of transonic flow over an axisymmetric bump with shock-induced separation," AIAA Paper 2017-3953, 2017.

[19] Gritskevich, M., Garbaruk, A., and Menter, F., "A comprehensive study of improved delayed detached eddy simulation with wall functions," *Flow, Turbulence and Combustion*, Vol. 98, No. 2, 2017, pp. 461–479.

[20] Fukushima, Y., and Kawai, S., "Wall-modeled large-eddy simulation of transonic airfoil buffet at high Reynolds number," *AIAA Journal*, Vol. 56, No. 6, 2018, pp. 2372–2388.

[21] Kiris, C. C., Stich, D., Housman, J. A., Kocheemoolayil, J. G., Barad, M. F., and Cadieux, F., "Application of Lattice Boltzmann and Navier-Stokes methods to NASA's wall mounted hump," AIAA Paper 2018-3855, 2018.

[22] Mettu, B. R., and Subbareddy, P. K., "Wall modeled LES of compressible flows at non-equilibrium conditions," AIAA Paper 2018-3405, 2018.

[23] Gonzalez, D. R., Adler, M. C., and Gaitonde, D. V., "Large-Eddy Simulation of Compressible Flows with an Analytic Non-Equilibrium Wall Model," AIAA Paper 2018-0835, 2018.

[24] Iyer, P. S., and Malik, M. R., "Large-eddy simulation of axisymmetric compression corner flow," AIAA Paper 2018-4031, 2018.

[25] Mettu, B. R., and Subbareddy, P. K., "Modeling non-equilibrium effects in wall modeled LES of high-speed flows," AIAA Paper 2019-3699, 2019.

[26] Gao, W., Zhang, W., Cheng, W., and Samtaney, R., "Wall-modelled large-eddy simulation of turbulent flow past airfoils," *Journal of Fluid Mechanics*, Vol. 873, 2019, pp. 174–210.

[27] Williams, O., Samuell, M., Sarwas, E. S., Robbins, M., and Ferrante, A., "Experimental study of a CFD validation test case for turbulent separated flows," AIAA Paper 2020-0092, 2020.

[28] Uzun, A., and Malik, M. R., "Simulation of a Turbulent Flow Subjected to Favorable and Adverse Pressure Gradients," AIAA SciTech 2020(Submitted), 2020.

[29] Khalighi, Y., Ham, F., Nichols, J., Lele, S., and Moin, P., "Unstructured large eddy simulation for prediction of noise issued from turbulent jets in various configurations," AIAA Paper 2011-2886, 2011.

[30] Park, G. I., and Moin, P., "Numerical aspects and implementation of a two-layer zonal wall model for LES of compressible turbulent flows on unstructured meshes," *Journal of Computational Physics*, Vol. 305, 2016, pp. 589–603.

[31] Kawai, S., and Larsson, J., "Wall-modeling in large eddy simulation: length scales, grid resolution, and accuracy," *Physics of Fluids (1994-present)*, Vol. 24, No. 1, 2012, p. 015105.

[32] Slotnick, J. P., "Integrated CFD validation experiments for prediction of turbulent separated flows for subsonic transport aircraft," NATO Science and Technology Organization, Meeting Proceedings RDP, STO-MP-AVT-307, 2019.

[33] Shur, M. L., Spalart, P. R., Strelets, M. K., and Travin, A. K., "Synthetic turbulence generators for RANS-LES interfaces in zonal simulations of aerodynamic and aeroacoustic problems," *Flow, Turbulence and Combustion*, Vol. 93, No. 1, 2014, pp. 63–92.

[34] Iyer, P. S., and Malik, M. R., "Analysis of the equilibrium wall model for high-speed turbulent flows," *Physical Review Fluids*, Vol. 4, No. 7, 2019, p. 074604.

[35] Iyer, P. S., and Malik, M. R., "Wall-modeled LES of the NASA juncture flow experiment," AIAA Paper 2020-1307, 2020.

[36] Yang, X. I., Park, G. I., and Moin, P., "Log-layer mismatch and modeling of the fluctuating wall stress in wall-modeled large-eddy simulations," *Physical review fluids*, Vol. 2, No. 10, 2017, p. 104601.

[37] Biedron, R. T., Carlson, J. R., Joseph, M. D., Gnoffo, P. A., Hammond, D. P., Jones, W. T., Kleb, B., Lee-Rausch, E. M., Nielsen, E. J., Park, M. A., Rumsey, C. L., Thomas, J. L., and Wood, W. A., "FUN3D manual: 13.1," NASA-TM-2019580, 2017.

[38] Spalart, P. R., "Strategies for turbulence modelling and simulations," *International Journal of Heat and Fluid Flow*, Vol. 21, No. 3, 2000, pp. 252–263.